CHAPTER VII

OBSERVED AND COMPUTED GROUND AND STRUCTURAL MOVEMENTS

Literature of different kinds of TBMs, tunneling methods, the general geological conditions of Bangkok and the detail of subsoil profiles including their engineering properties at the selected locations are reviewed in the previous chapters to establish the background of this research. Moreover, the causes and the methods for predicting ground movements induced by tunnel excavation as well as the analysis method of the present study have been extensively described. This chapter explains the various results obtained from FE back-analyses and the results based on empirical method for surface settlements. The description of the behaviors of ground surface and subsurface movements in response to the advancement of EPB shield, and the interpretation of the analysis results as well as some discussions are also presented in this chapter. In addition, the internal forces of segmental lining resulted from FE analyses are also mentioned.

7.1. Ground Movements

The computed results based on FE program and the monitored data for ground surface and subsurface settlements will be compared in this section. Figures 7.1 and 7.2 show the input geometries of the different analysis sections at Klongtan Bridge and BTS-Sukhumvit areas, respectively. The global mesh for all the analysis sections is very fine; moreover, the mesh refinement is also applied to the clusters inside the tunnel. The examples of finite element mesh generated at section AA cut along GS16 and at section BB (GS35) are illustrated in Figures 7.3 and 7.4, respectively. The generated mesh along GS16 (section AA) at Klongtan Bridge area consists of 4 603 elements, 37 403 nodal points and 55 236 stress points while the mesh of section BB (GS35) is composed of 3 169 elements, 25 815 nodal points and 38 028 stress points. However, the criteria of finite element mesh depend mainly on the types of elements

selected for the input program, the dimension of model to simulate, and the input of existing structures. Some graphical input and output are shown in Appendix D.

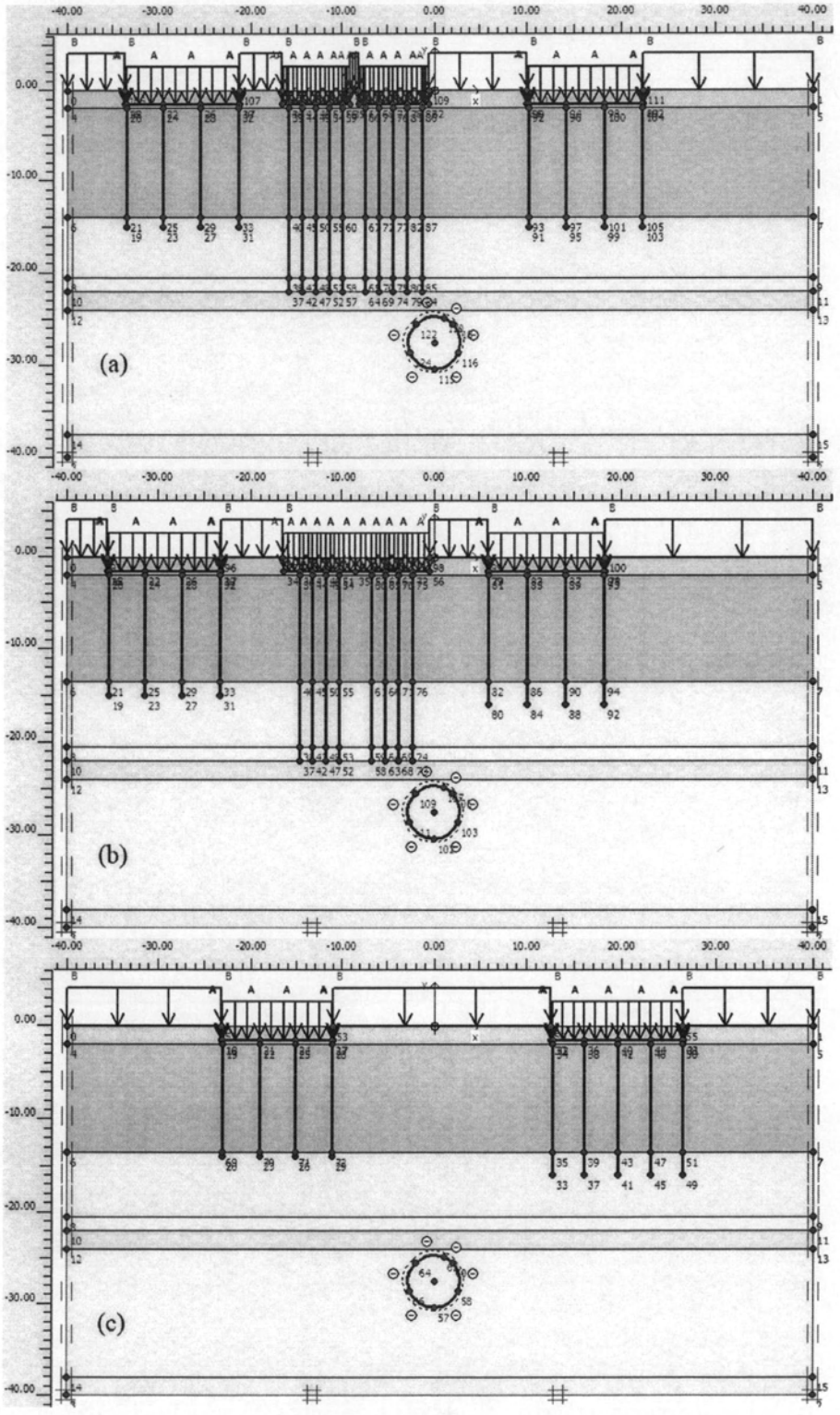

Figure 7.1 Input geometries of different analysis sections at Klongtan Bridge area; (a) GS16, (b) GS17 and (c) GS18

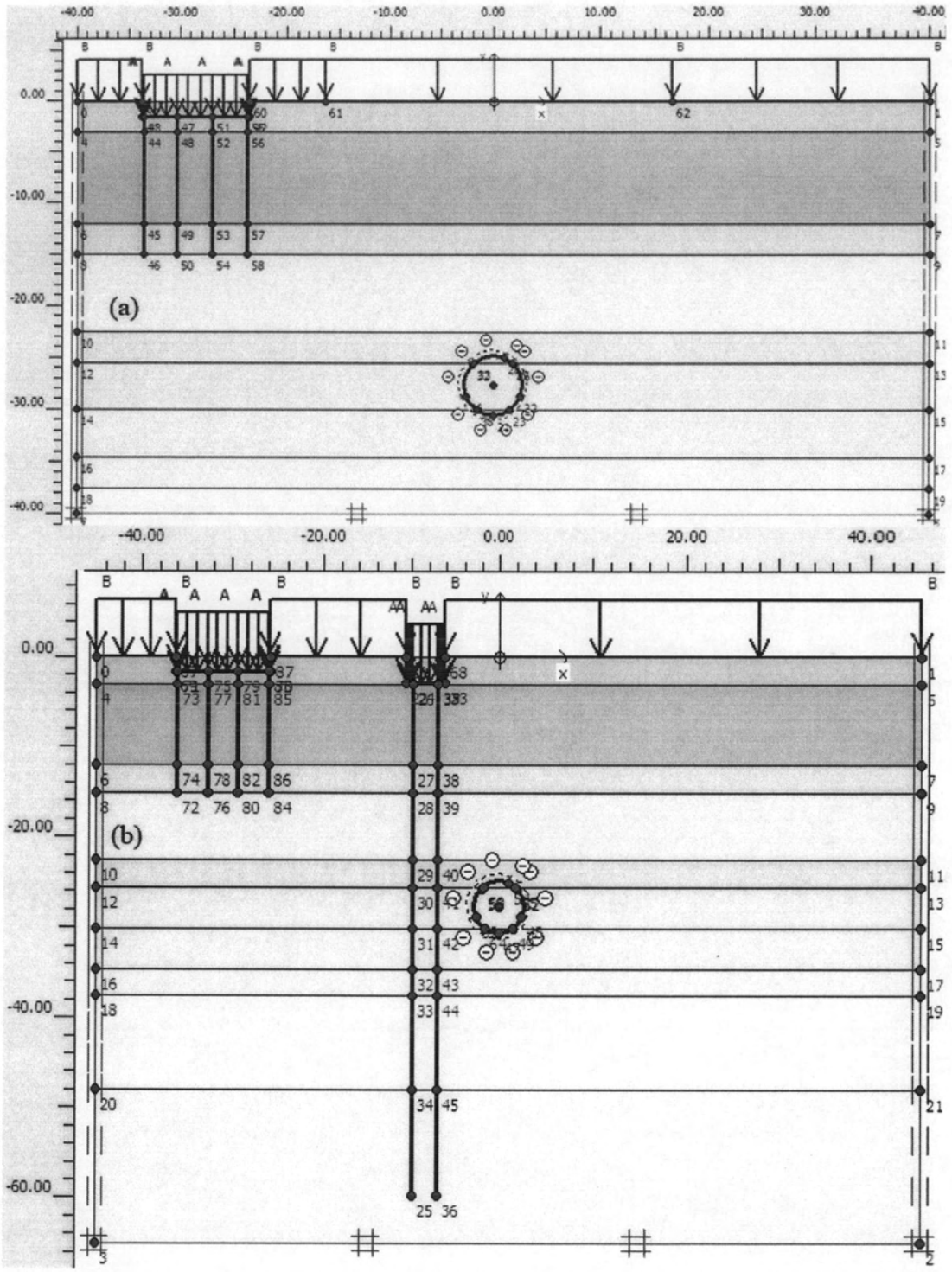

Figure 7.2 Input geometries of different analysis sections at BTS-Sukhumvit area; (a) GS-BTS and (b) GS35

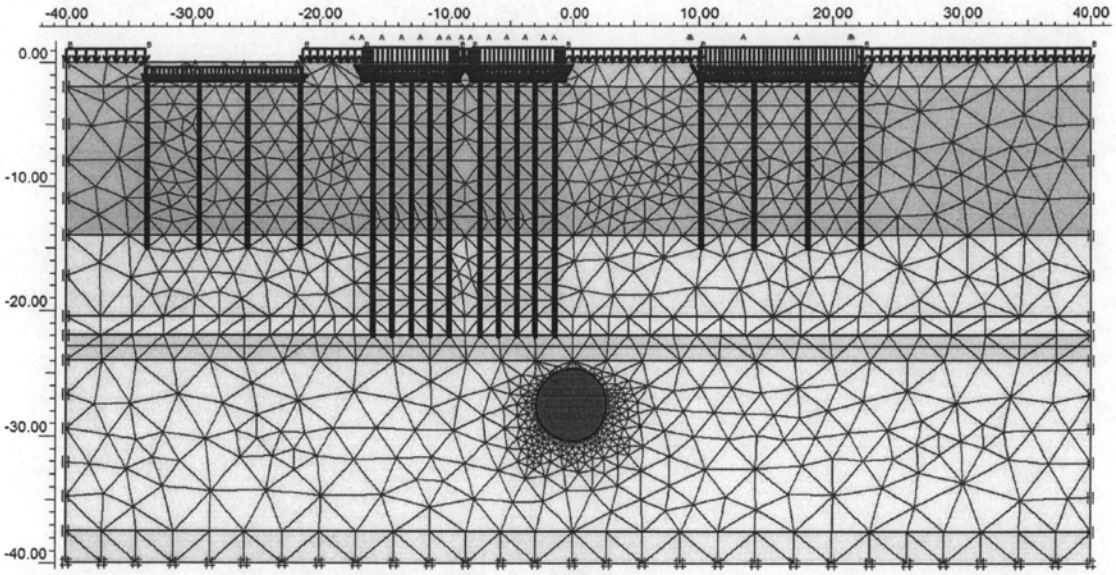

Figure 7. 3 Finite element mesh generated at section AA (Klongtan Bridge area)

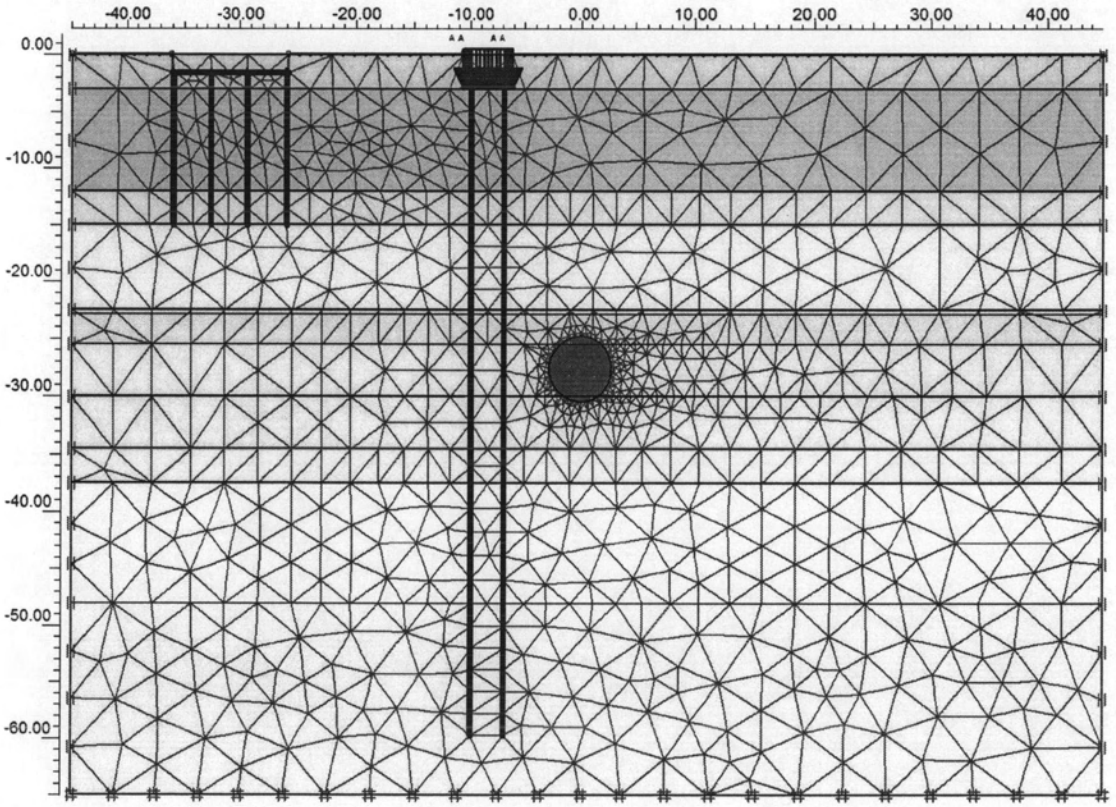

Figure 7.4 Finite element mesh generated at section BB (BTS-Sukhumvit area)

7.1.1. Behaviors of Ground Surface and Subsurface Deformation

The behaviors of the recorded ground surface and subsurface deformation at Klongtan Bridge and BTS-Sukhumvit area can be classified into 3 phases (Figures 7.5 and 7.6): deformation in front shield face, deformation within the length of shield body when the cutting face has been passed and the deformation behind the shield which consists of tail void deformation and subsequent settlement. As mentioned in section 4.1.2 of Chapter IV, the deformation in front of the shield is mainly caused by the decline of groundwater table in silty sand and the imbalance of total pressure at the TBM face. Friction between shield machine and surrounding soil or disturbance of the ground due to the over-excavation causes the deformation within the shield length. However, the deformation behind the tail of shield is due to the effects of tail void or excessive grouting pressure.

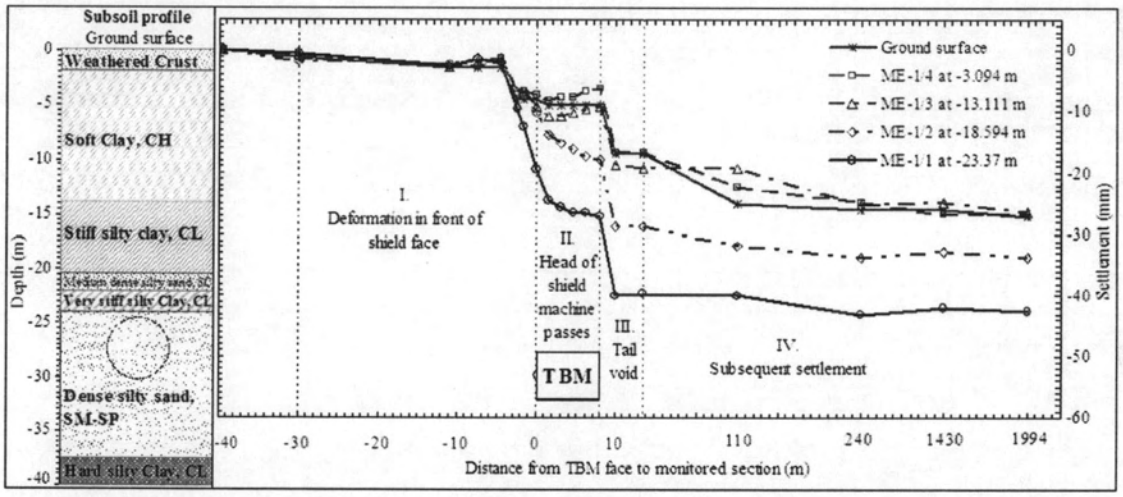

Figure 7.5 Behaviors of surface and subsurface deformation at extensometer ME-1 (Klongtan Bridge area)

The gradual settlements are found for the tunnel construction in dense silty sand at Klongtan Bridge area, and these settlements are rapidly increasing when the shield approaches close to the controlled section. The vertical movements slightly appear again for the whole shield body, and then a brutal settlement at the tail of the shield shows and remains constant during the tail void grouting. The settlements of all the layers seem constant after about one week when the TBM passes the monitored section (110 m. in Figure 7.5). The vertical deformations responding to the shield

movements of the tunnel located in hard silty clay are different from those in dense silty sand because they fluctuate within the first and second portions. Nevertheless, the settlements become more or less constant about one week after TBM passes as well (107 m. in Figure 7.6).

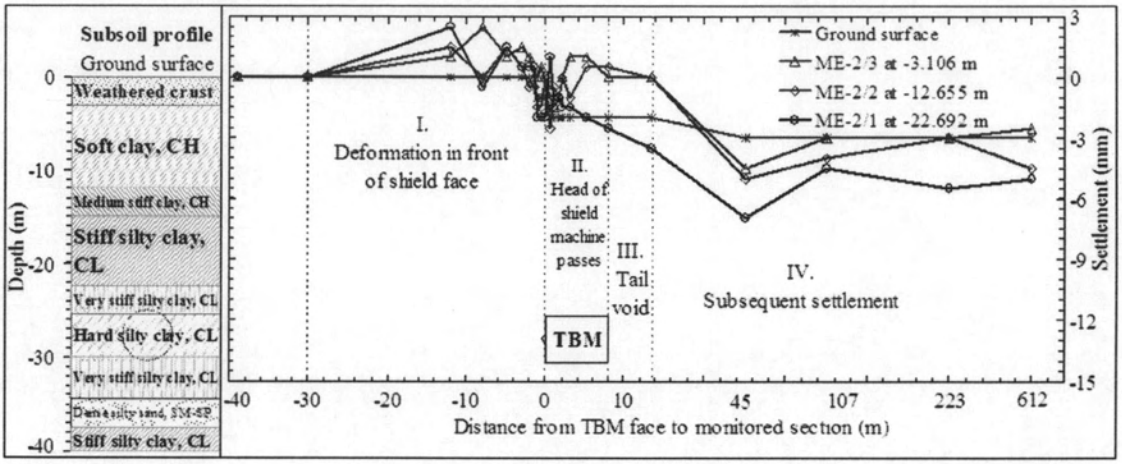

Figure 7.6 Behaviors of surface and subsurface deformation at extensometer ME-2 (BTS-Sukhumvit area)

It is noticeable when the tunnel is excavated in dense silty sand, the ground settlements corresponding to the positions of the face and tail of the TBM accelerate with average settlements about 42% and 77%, respectively, of the total settlement measured after three months. While in hard silty clay, these settlements reduce to 18% and 35 % respectively. In both cases, the average magnitude of settlement one week after the pass of the TBM reaches to 90% of the settlement after three months, which could be considered as the final short-term settlement.

7.1.2. Ground Surface Settlements

By reproducing the settlement trough based on the empirical method (Equations 4.1 and 4.6), the volume of ground loss resulting from the tunnel excavated in the dense silty sand layer at Klongtan Bridge area is 1.79% for the monitored sections GS16 and GS18 (Figure 7.7a and c). However, this ground loss is slightly increased to 1.97% for the section GS17, which is located close to the toe of the bridge. The figures show a good agreement among empirical and numerical

results and the measured data (obtained three-month after TBM passes). The values of i are $0.24z_0$, $0.26z_0$ and $0.35z_0$ for events as in Figures 7.7a, 7.7b and 7.7c respectively and where z_0 is the depth from the ground surface to the tunnel axis.

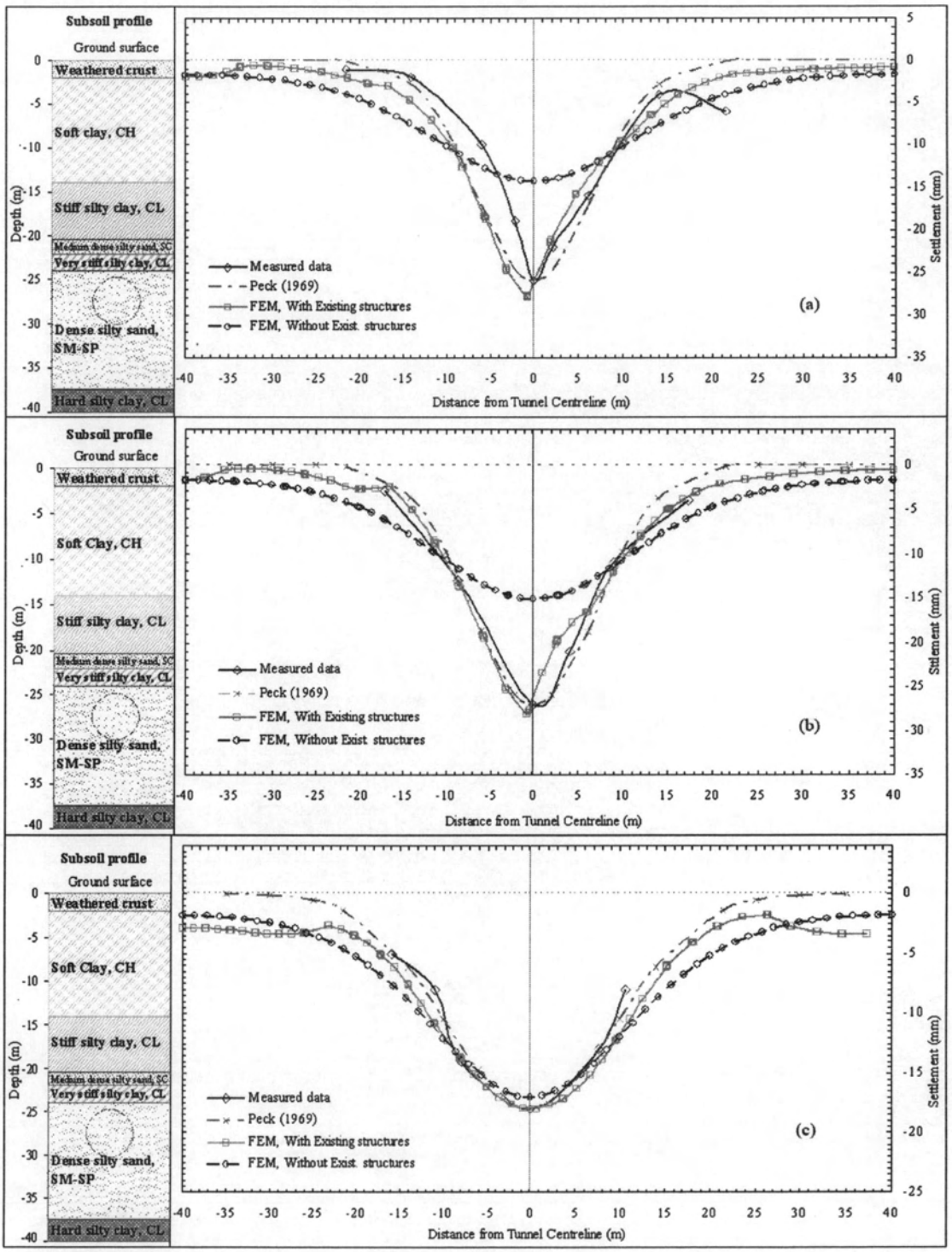

Figure 7.7 Surface settlements monitored and computed at Klongtan Bridge area; (a) GS16, (b) GS17 and (c) GS18

In the same way as at Klongtan Bridge area, the surface settlement troughs at BTS-Sukhumvit area (tunnel in hard silty clay) are replicated (Figure 7.8). Based on the same empirical equations (Equations 4.1 and 4.6), the volume of ground loss of Figure 7.8a is 0.77% where the ground surface settlement points are implanted into the pavement of busy road at the curvature (GS-BTS, Figure 5.4). Consequently, the empirical prediction is in good agreement with the measured and finite element displacements. Unfortunately, the empirical result cannot agree with the measured data which are monitored along a line so close to the BTS foundation (about 2 m) while numerical result only shows an agreement in deformation shape (Figure 7.8b). Only three points are observed for this settlement array, and the middle point is implanted about 10 cm close to the curve in the middle of the road. The value of i is $0.46z_0$ for events as in Figure 7.8a.

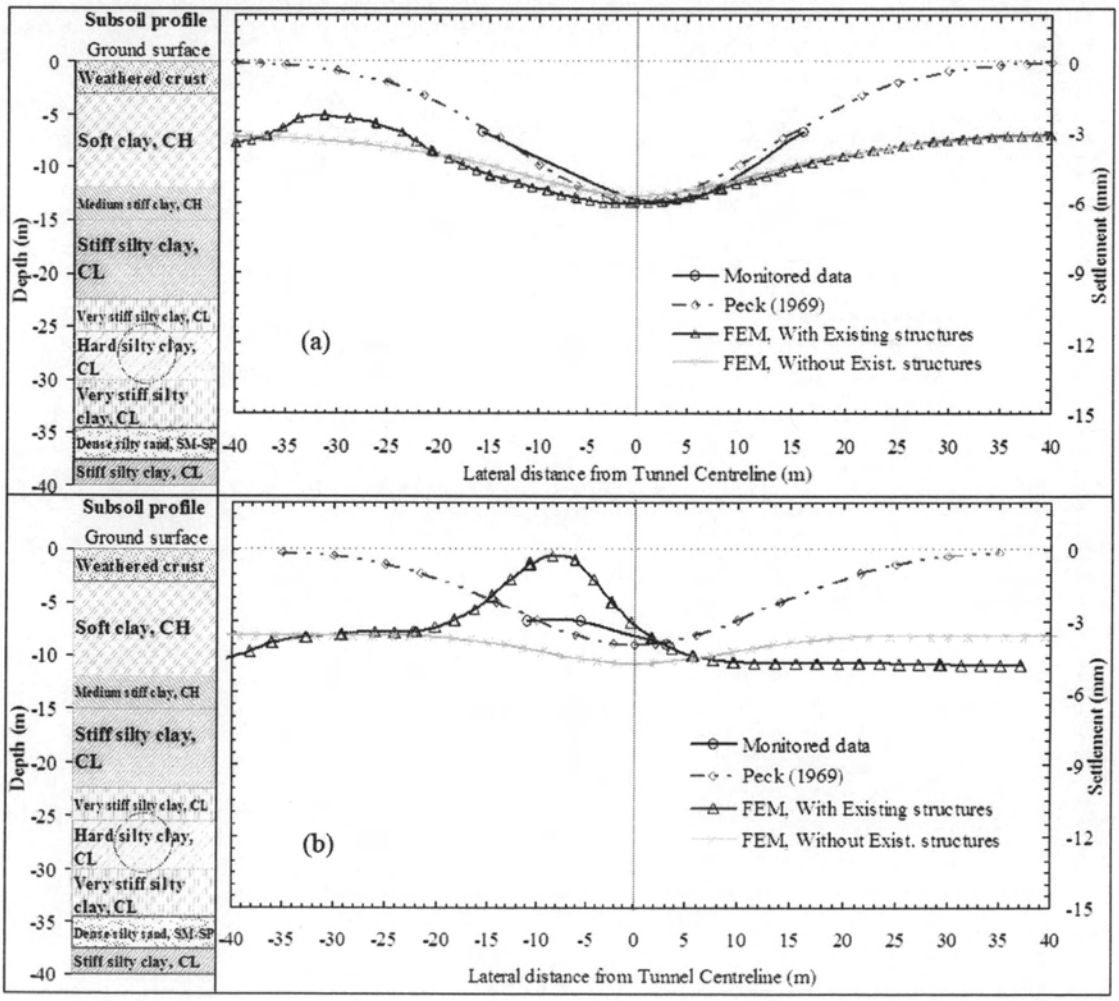

Figure 7.8 Surface settlements monitored and computed at BTS-Sukhumvit area (a) GS-BTS and (b) GS35

7.1.3. Subsurface Settlements

To monitor the subsurface settlements, two borehole extensometers are placed above the tunnel center line at Klongtan Bridge and BTS-Sukhumvit areas (Figures 5.6 and 5.7). The magnitude of subsurface settlement obtained after a three-month pass of TBM gradually increases toward the crown of the tunnel as shown in Figures 7.9 and 7.10. These two figures also show the comparison between the monitored data and the values given by the FEM. A good agreement is observed between field measured data and numerical results.

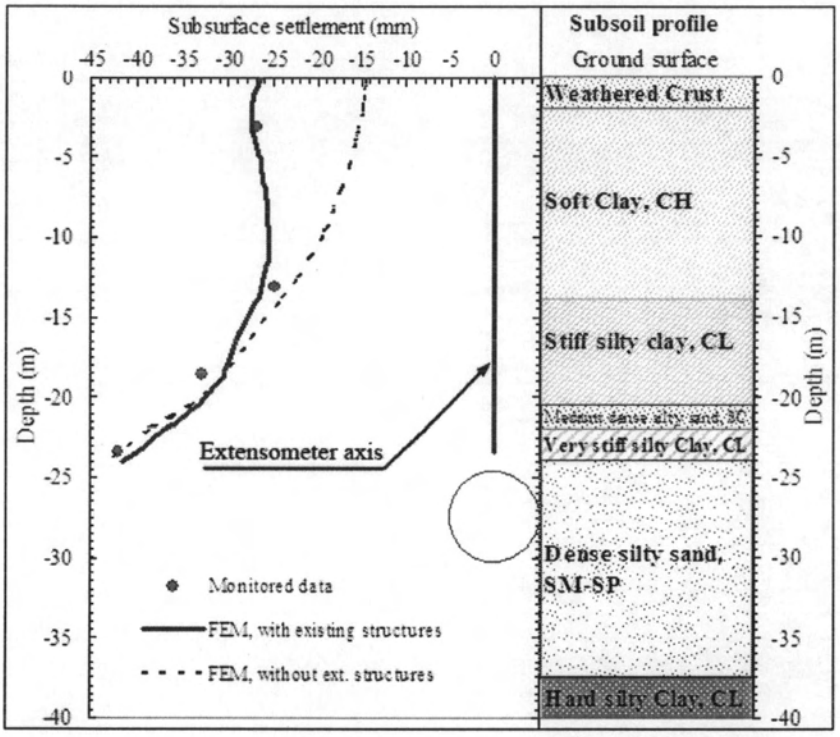

Figure 7.9 Subsurface settlements along Extensometer ME-1 at Klongtan Bridge area

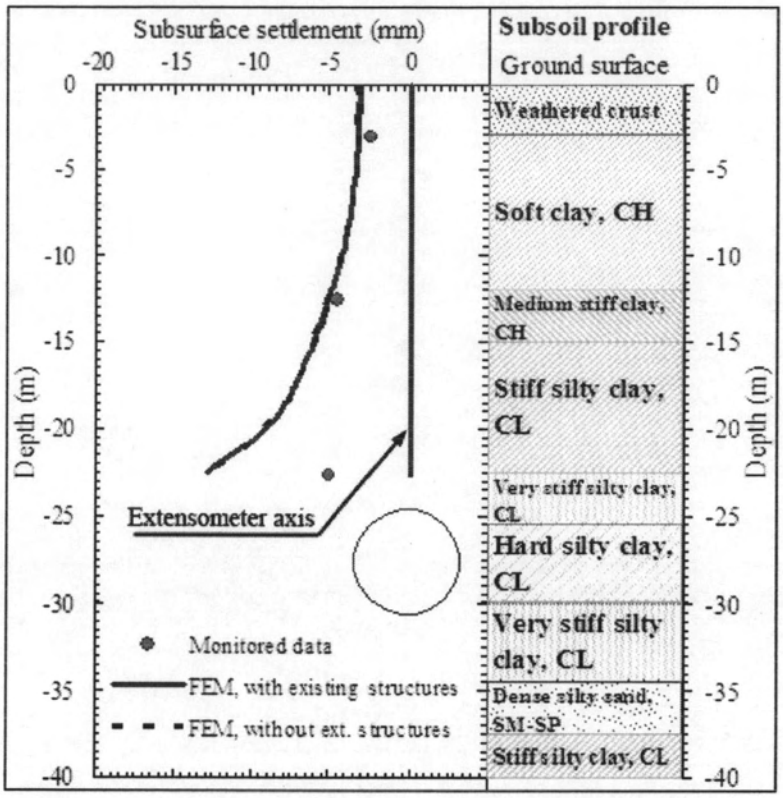

Figure 7.10 Subsurface settlements along Extensometer ME-2 at BTS-Sukhumvit area

7.1.4. Lateral Displacements

Figure 7.11 shows the lateral deformations monitored by means of an inclinometer at BTS-Sukumvit area (Figure 5.4) responding to different positions of the TBM face. It is apparent when the TBM face is 12 m away from the monitored station, the lateral displacement is slightly moved toward the tunnel axis. This movement can possibly be caused by the low pressure applied to the TBM face. However, the movement gradually occurs outward the tunnel axis when the TBM face arrives at 8 m away from the station and reaches a maximum outward displacement when the TBM face arrives at 2 m. After reaching the maximum outward lateral displacement, the soil starts to move inward until a maximum when the TBM face is located at the monitored station, and then the inward lateral displacement reduces a few millimeters at the tunnel spring line during and after the tail void grouting. The lateral displacement remains constant after the shield face passes 12 m away from the monitored section. All the lateral movements can be closely related to the degree of

soil disturbance as well as the pressure applied to the shield face and grout pressure. The comparison between the lateral displacement and the values given by the FE analysis is also presented in the figure. However, the lateral deformations given by FE analysis are less than the final short-term deformations measured after three months; the difference can be caused by the effect of large bored pile foundation stiffness next to the instrumentation as shown in Figure 5.4 of Chapter V.

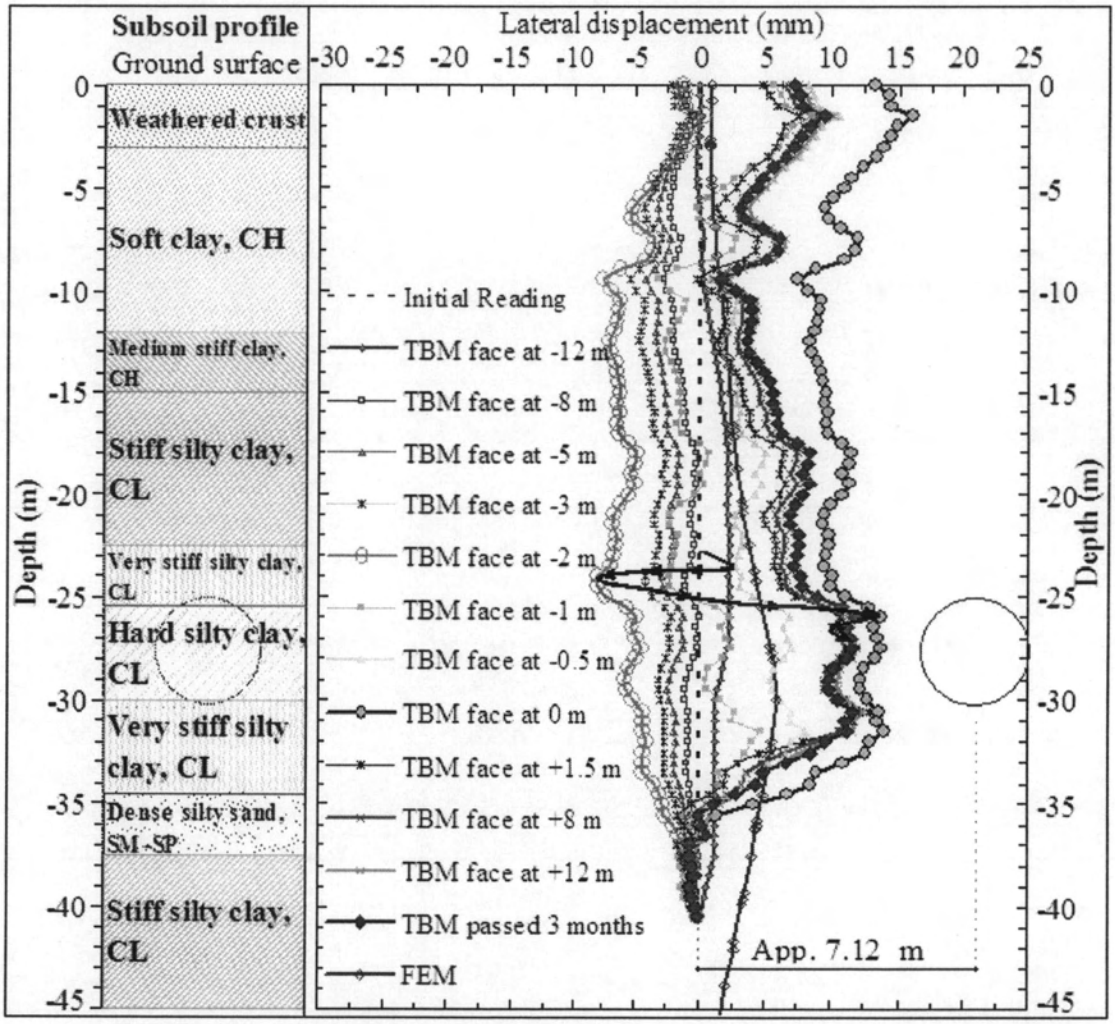

Figure 7.11 Lateral displacements caused by tunnel in hard silty clay at BTS-Sukhumvit area (Inclinometer, IC)

7.2. Structural Responses

As mentioned in section 5.2 of Chapter V, there are two important structures: old Klongtan Bridge and BTS sky train foundations at both studied areas and they are particularly monitored before, during and after the pass of EPB shield machine. However, no settlement is observed for the foundations of BTS sky train. The non-settlement of BTS sky train foundations can confirm that the tunnel excavation has no effect on the bored piles (diameter of each pile is one meter) of those foundations, which are strongly embedded in a very dense sand layer with pile tips of about 60 m below ground surface.

The settlements of the old Klongtan Bridge pile foundations where the TBM passes about 3 meters underneath are recorded. However, the foundations in the canal are not in the scope of this study. The settlement points are fixed on the columns or on the beams of the bridge at different levels from ground surface. Figure 7.12 shows the locations of monitored points except point C, which is fixed on the bridge column at the same level as point D that is not mentioned. On the contrary, point H is monitored on the bridge component, which is located at ground surface level above the pile cap embedded in the soil (Figure 7.13). Except for the portion of the shield length, where the significant settlements are also observed, the behaviors of the bridge foundation settlements (Figure 7.14) are very similar to those of the ground movements described previously. The settlements almost stop one week after the TBM passes (108 m) as well.

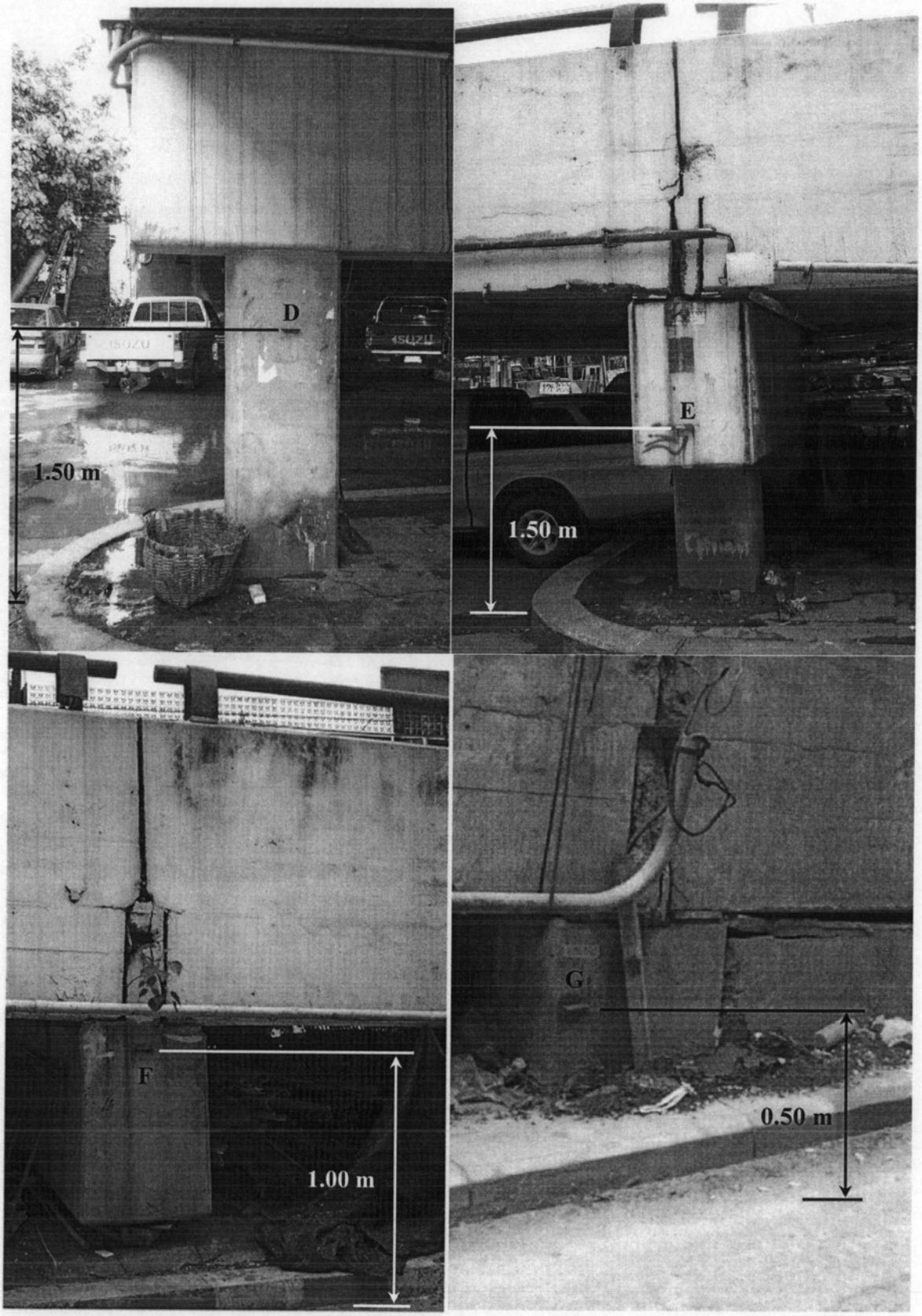

Figure 7.12 Location of structural settlement points monitored on Klongtan bridge

Figure 7.13 Location of point H monitored on Klongtan bridge

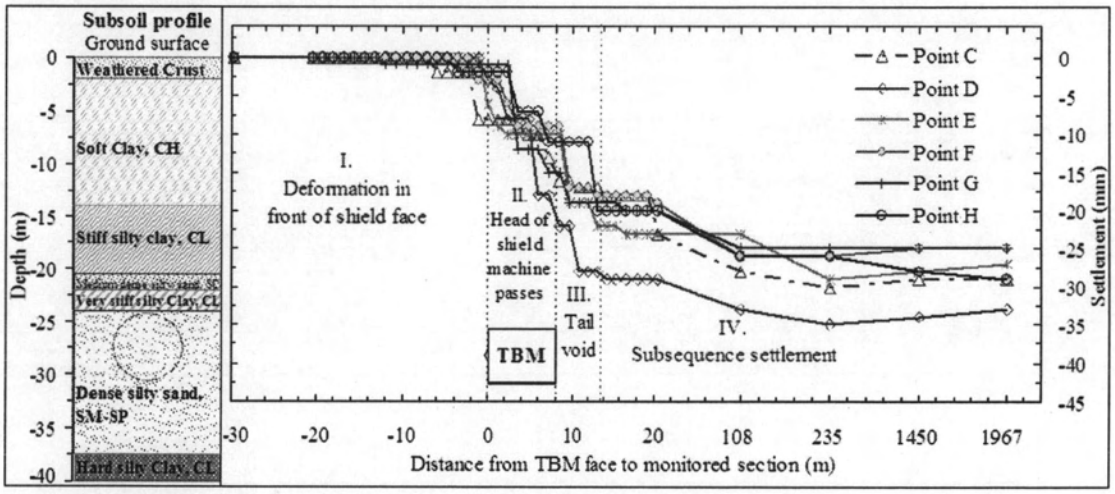

Figure 7.14 Behaviors of bridge foundation settlements caused by EPB tunneling in dense silty layer

In addition to the old bridge, some building settlement points are also placed to monitor the settlements of 3- and 4-storey old shophouses located on the right side of the bridge (Figure 5.2). The monitored points are placed on the columns of the shophouses about 1.50 m from the ground surface. However, only points C_1 and and

C_2, which are marked on the columns of the 3-storey shophouse, are shown in Figure 7.15.

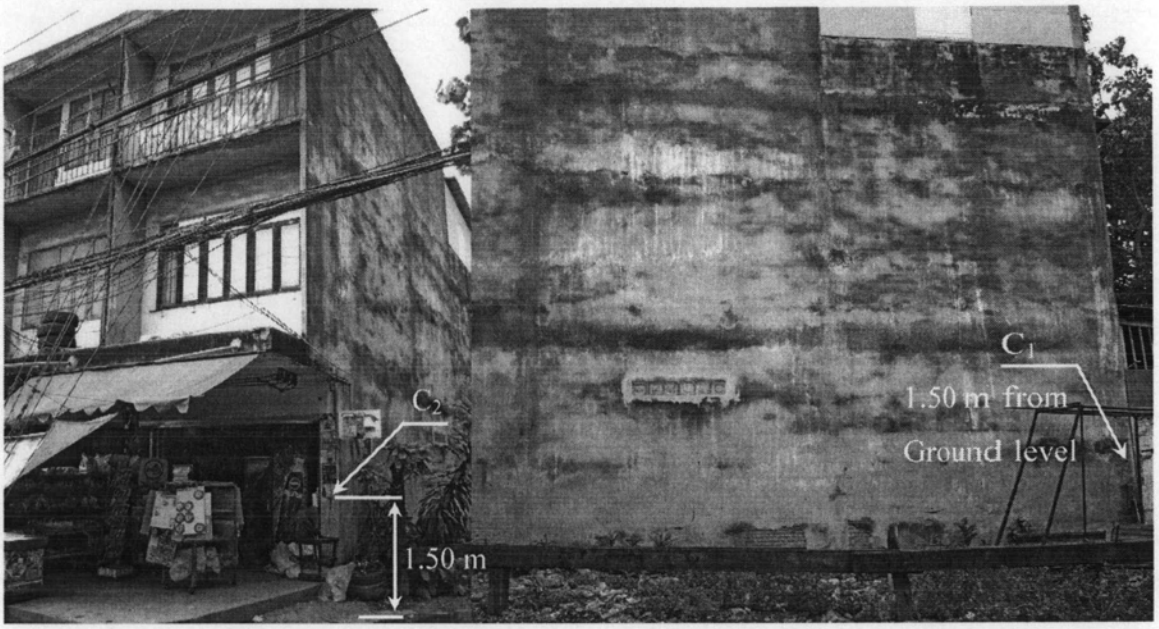

Figure 7.15 Location of point C_1 and C_2 monitored on 3-storey shophouse

The behaviors of the old shophouse settlements in response to the position of the cutting face of EPB shield machine are plotted in Figures 7.16 and 7.17. Similarly to the old Klongtan Bridge, the settlements are almost dissipated after the TBM passes about one week (106 m) from the monitored sections. Since the magnitude of the settlements of old shophouses are generally smaller than that of the bridge, the bridge settlement gained more attention at this point. Therefore, the monitoring of the old shophouse settlements is not continued after the TBM moves away about two weeks from the controlling sections.

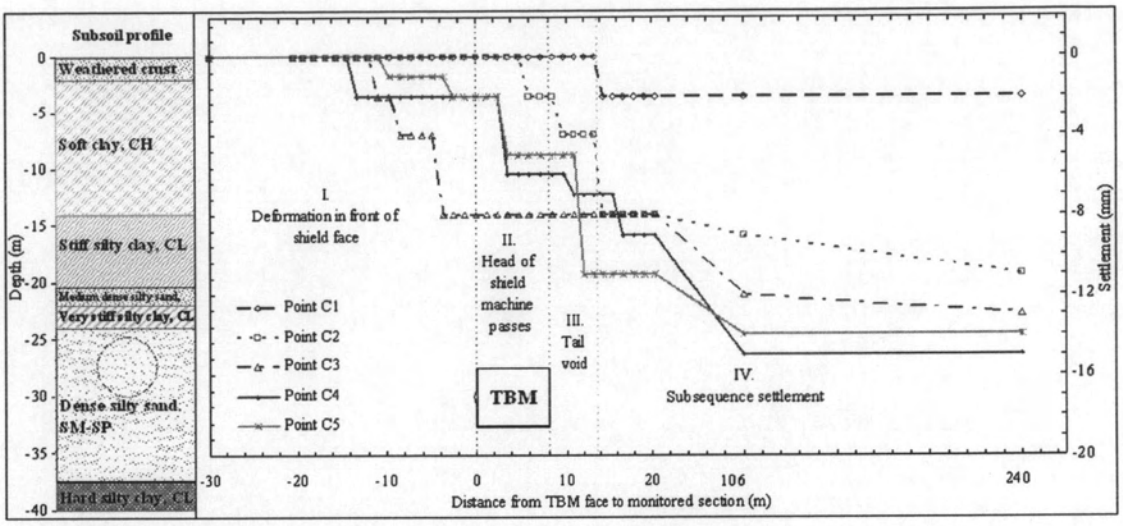

Figure 7.16 Behaviors of 3-storey old shophouse settlements in response to EPB tunneling in dense silty layer

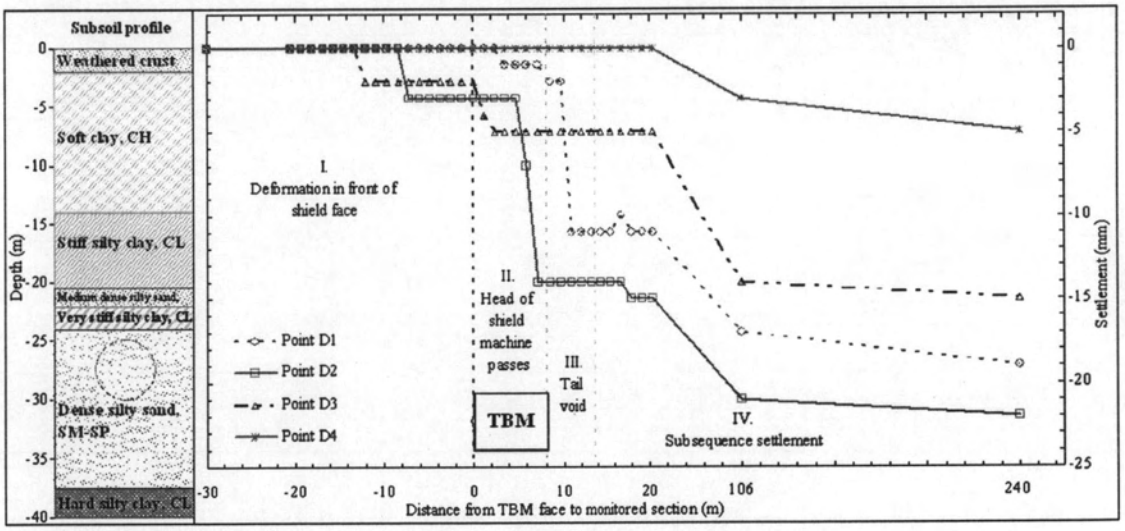

Figure 7.17 Behaviors of 4-storey old shophouse settlements in response to EPB tunneling in dense silty layer

As mentioned in Chapter VI, the analysis configurations of each bridge footing and the existing old shophouses based on 2D FEM are the same whereas only the positions of the structures to the tunnel center line are adjusted according to the real analysis sections. The magnitudes of old bridge and shophouse settlements are listed in Table 7.1. The 2D-FEM results are well comparable with the monitored data.

Table 7.1 Magnitude of structural settlements at Klongtan Bridge area

Structure	Source of data	Magnitude of settlement points					
Bridge foundation		C	D	E	F	G	H
	Monitored data	-29	-34	-28	-25	-25	-28
	2D-FEM results	-30.3	-30.8	-29.9	-25.9	-24.1	-28.2
3-storey old		C_1	C_2	C_3	C_4		
shophouse	Monitored data	-2	-11	-13	-15		
	2D-FEM results	-1.6	-9.8	-12.2	-16.7		
4-storey old		D_1	D_2	D_3	D_4		
shophouse	Monitored data	-19	-22	-15	-5		
	2D-FEM results	-17	-17.8	-17.3	-3.09		

7.3 Internal Forces of Segmental Lining

In addition to deformations given by PLAXIS after a completed analysis, various output parameters can be also investigated. However, this section focuses only on the internal forces of tunnel lining. These forces appear as a result of the water pressure, overburden pressure and loads which are transmitted from the surcharges at ground surface. For sign conventions used in PLAXIS, please refer to section 6.1.1 of Chapter VI.

Figure 7.18 shows the bending moments in tunnel lining at the final phase of simulation for the section GS16, where the tunnel is excavated in dense silty sand layer. The lining carries a positive bending moment of 151.78 kNm/m at the crown and 133.24 kNm/m at the invert, but the negative bending moment of -106.33 kNm/m and -119.62 kN/m at the left and right springline, respectively. Therefore, the extreme value of bending moment is located at crown.

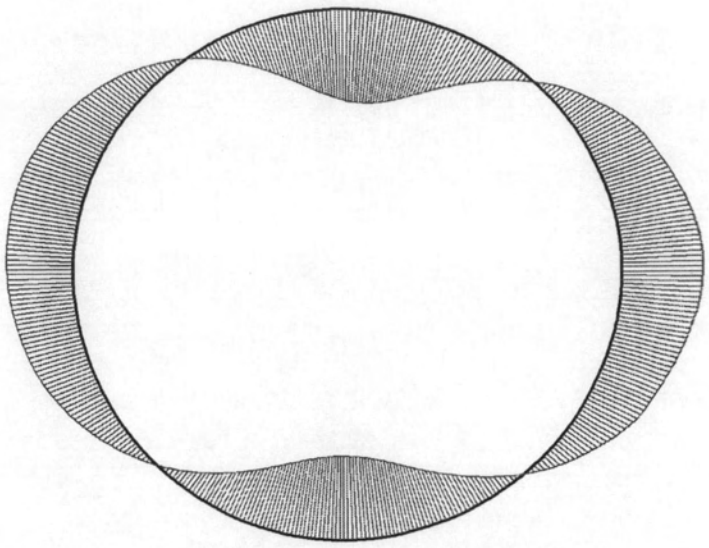

Figure 7.18 Bending moments in the tunnel lining at the final phase of simulation for section GS16, the extreme bending moment is 151.78 kNm/m

In addition, the results of axial and shear forces are presented in Figures 7.19 and 7.20. The highest compressive axial force of -510.18 kN/m is located at the springline on the right side while on the left side the axial force is only -484.83 kN/m. The maximum shear force of 115.31 kN/m is located at the right shoulder of the tunnel lining.

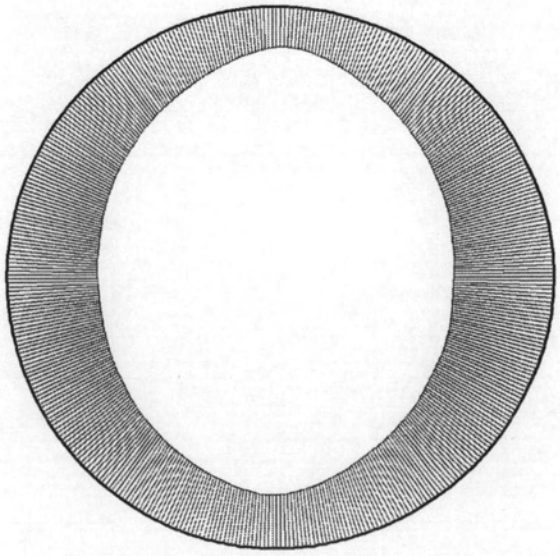

Figure 7.19 Axial forces in the tunnel lining at the final phase of simulation for section GS16, the extreme axial force is -510.18 kNm/m

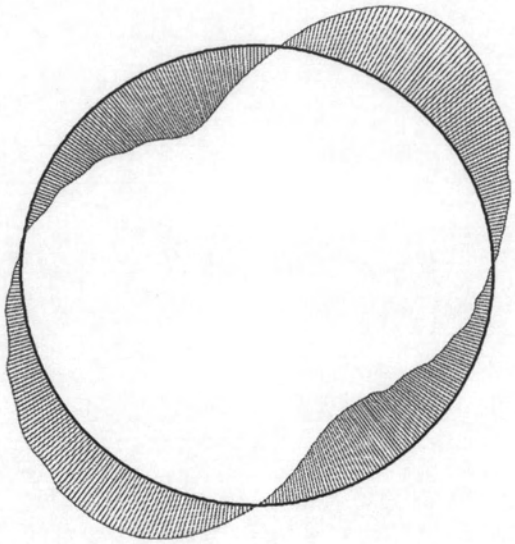

Figure 7.20 Shear forces in the tunnel lining at the final phase of simulation for section GS16, the extreme shear force is 115.31 kNm/m

Based on the same subsoil profile, Figures 7.21 to 7.26 show the axial forces, shear forces and bending moments generated in the tunnel lining at the final phase of simulation for the section GS17 and GS18. Some remarkable values of axial forces, shear forces and bending moments as well as their locations on the tunnel lining for both sections are listed below:

- The maximum compressive axial forces of -505.34 kN/m and -485.61 kN/m are located at the springline on the right and left side for sections GS17 and GS18, respectively.
- The extreme shear forces of 113.49 kN/m and 109.52 kN/m are located at the right shoulder of the tunnel lining for both sections GS17 and GS18.
- The extreme positive bending moments of 155.27 kNm/m and 150.42 kNm/m for both cases are located at the crown of the tunnel.

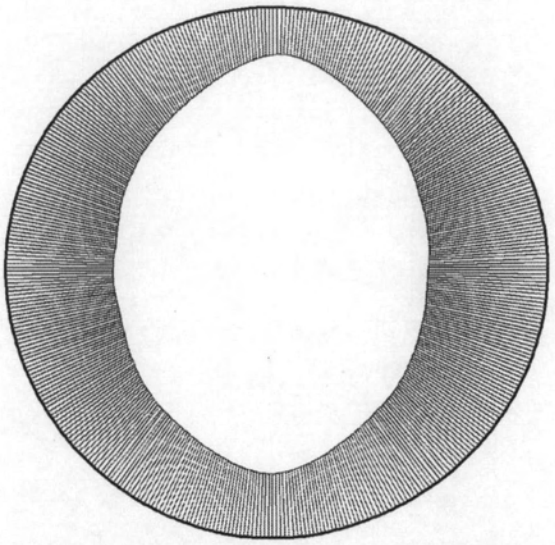

Figure 7.21 Axial forces in the tunnel lining at the final phase of simulation for section GS17, the extreme axial force is -505.34 kNm/m

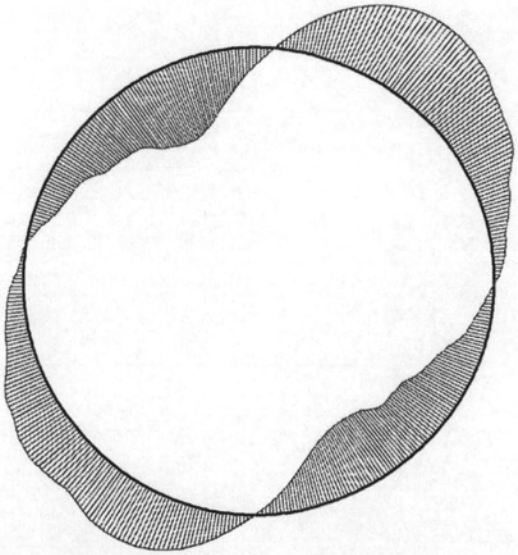

Figure 7.22 Shear forces in the tunnel lining at the final phase of simulation for section GS17, the extreme shear force is 113.49 kNm/m

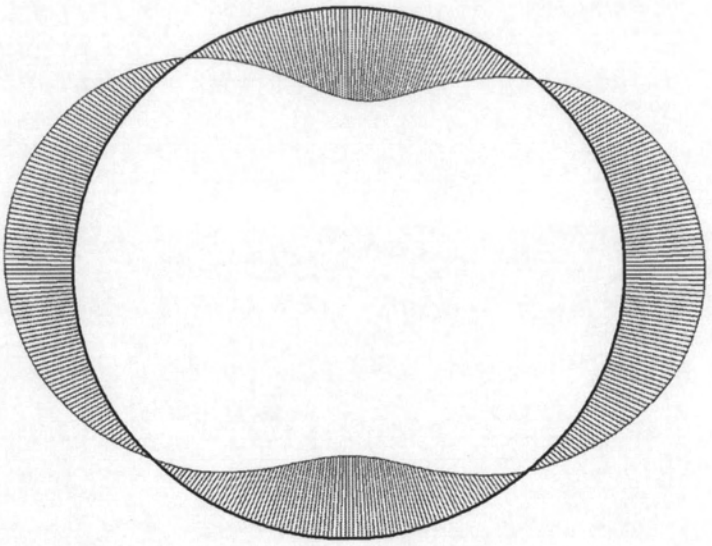

Figure 7.23 Bending moments in the tunnel lining at the final phase of simulation for section GS17, the extreme bending moment is 155.27 kNm/m

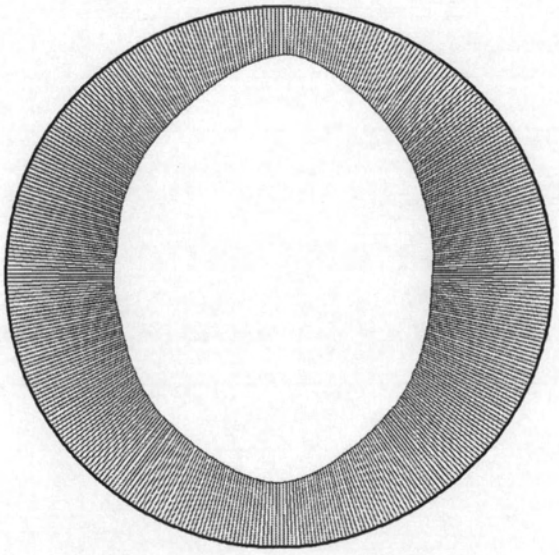

Figure 7.24 Axial forces in the tunnel lining at the final phase of simulation for section GS18, the extreme axial force is -485.61 kNm/m

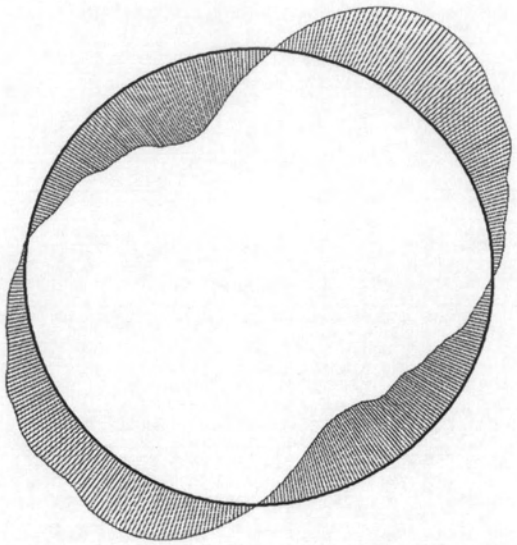

Figure 7.25 Shear forces in the tunnel lining at the final phase of simulation for section GS18, the extreme shear force is 109.52 kNm/m

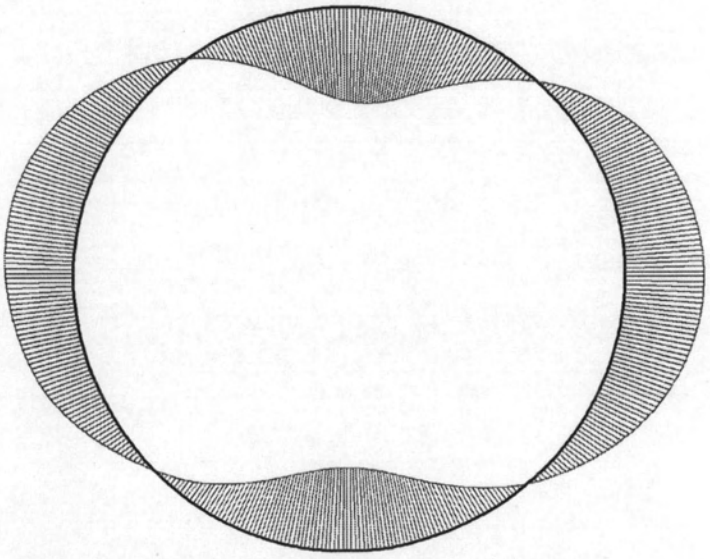

Figure 7.26 Bending moments in the tunnel lining at the final phase of simulation for section GS18, the extreme bending moment is 150.42 kNm/m

Among the three cases of tunnel in dense silty sand layer, the axial and shear forces as well as the bending moments in lining for the tunnel located under the road imprisoned by the pile foundations of two-storey residential houses and four-storey shophouses on the left and right sides (GS18, Figures 7.24 to 7.26) are lower than

those for the tunnel located below the bridge. These clearly show that the loads transmitted from both side of houses and shophouses to the tunnel lining are less than those of the bridge.

In the case where the tunnel is bored through the hard silty clay with the crown and invert cut in the very stiff silty clay layers (GS-BTS and GS35), the forces and bending moments generated in the tunnel lining are shown in Figures 7.27 to 7.32. A description of the extreme forces and bending moments for the two selected sections can be summarized as:

- The maximum compressive axial forces of -439.08 kN/m and -370.15 kN/m are located at the springline on the left and right side for sections GS-BTS and GS35, respectively.
- The extreme shear forces of 129.82 kN/m and -142.78 kN/m are located on left and right sides between the springline and the invert of the tunnel lining for both sections GS-BTS and GS35, respectively.
- The extreme positive bending moments of -132.43 kNm/m and -147.08 kNm/m at the left and right springline of the tunnel lining for both sections GS-BTS and GS35, respectively.

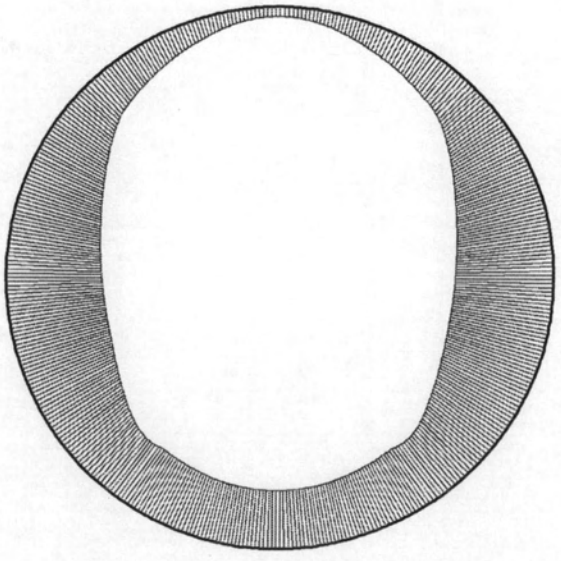

Figure 7.27 Axial forces in the tunnel lining at the final phase of simulation for section GS-BTS, the extreme axial force is -439.08 kNm/m

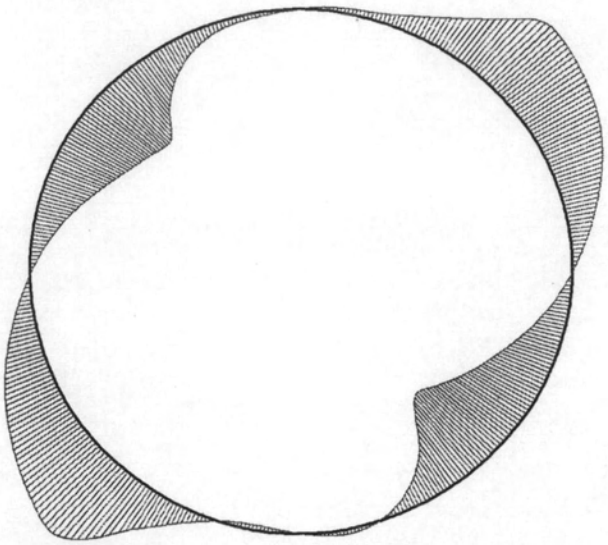

Figure 7.28 Shear forces in the tunnel lining at the final phase of simulation for section GS-BTS, the extreme shear force is 129.82 kNm/m

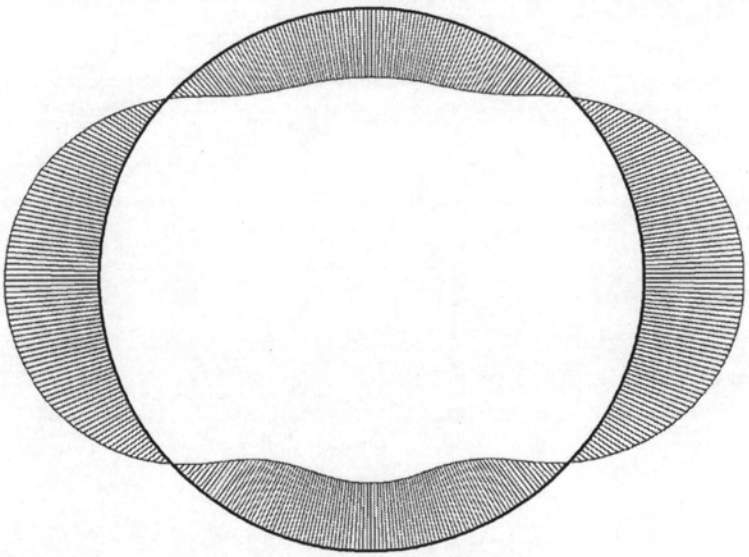

Figure 7.29 Bending moments in the tunnel lining at the final phase of simulation for the section GS-BTS, the extreme bending moment is -132.43 kNm/m

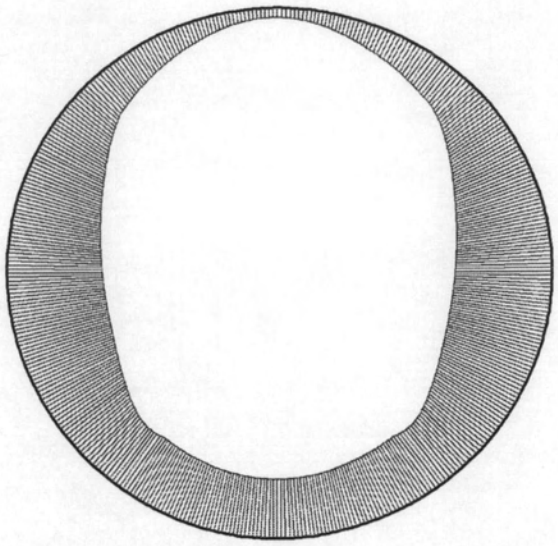

Figure 7.30 Axial forces in the tunnel lining at the final phase of simulation for section GS35, the extreme axial force is -370.15 kNm/m

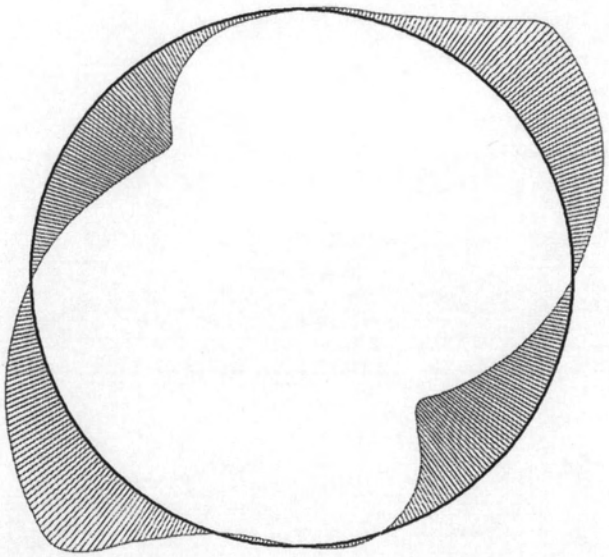

Figure 7.31 Shear forces in the tunnel lining at the final phase of simulation for section GS35, the extreme shear force is -142.78 kNm/m

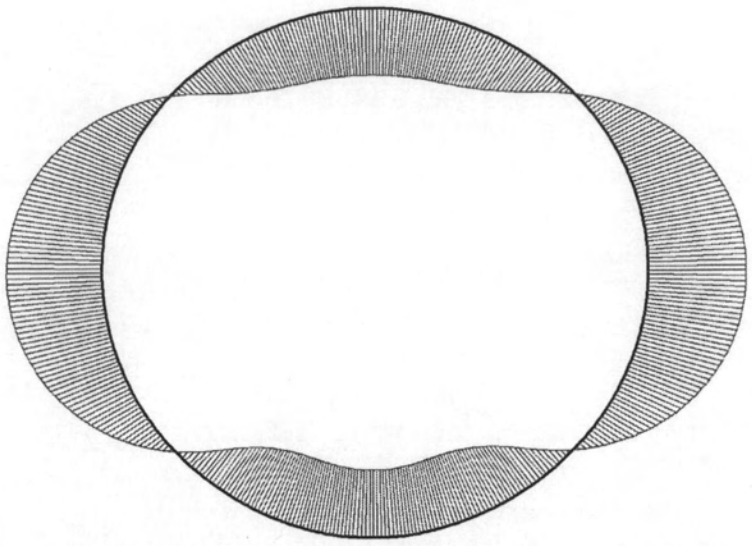

Figure 7.32 Bending moments in the tunnel lining at the final phase of simulation for section GS35, the extreme bending moment is -147.08 kNm/m

7.4. Discussion

7.4.1. Surface and Subsurface Deformation

Based on the longitudinal plots for ground surface and subsurface settlements, we observe that the significant settlement takes place at the specific positions of the shield, face and tail, especially for the subsoil layers which are in the zone of one diameter above the crown of the tunnel (ME-1/1 and ME-2/1 in Figures 7.5 and 7.6). It is probably a sensitive area. However between these two positions, some heaves are also observed for the tunnel excavated in hard silty clay layer. These also provide important information that the pressure at shield face and the grout pressure for a tunnel construction in clay layer have a remarkable effect on the surrounding soil than that for a tunnel construction in sand or silty sand layer, where the coefficient of permeability is usually high.

In addition, the magnitudes of ground surface settlement induced by tunnel in hard silty clay are 5 to 7 times smaller than settlements induced by tunnel in dense silty sand (Figures 7.7 and 7.8). It is probably because of the drawn down of groundwater level during the tunnel excavated in dense silty sand layer and the degree of disturbance of TBM in dense silty sand is higher than that in hard silty clay. For the similar reasons, the magnitude of subsurface settlements induced by tunnel in hard

silty clay is smaller than that of subsurface settlements induced by tunnel in dense silty sand (Figures 7.9 and 7.10). However, the differences of settlement magnitudes are increased up to 6 to 9 times higher for tunnel in dense silty sand than for tunnel in hard silty clay layer.

7.4.2. Effects of Existing Structures on FE Analysis

For the FE analysis, when building structures are added as a parameter, the results of the surface settlements are strongly influenced as shown in Figures 7.7 and 7.8. Therefore building structures are influential and they also are a factor to be considered in numerical analysis. When the existing structures are ignored from the analysis model, the magnitude of ground displacement will be underestimated. However, the influences of existing structures and their surcharges on subsurface settlements are reduced with depth as shown in Figure 7.8 except for Figure 7.9 where the existing three-storey shophouses are located about 30 m. from the monitored extensometer, which is implemented above the tunnel center line (Figure 5.6).

Moreover, the presence of different structures which are generally not uniform above the tunneling route leads to a non-uniform of charge repartition. Therefore, an asymmetry of ground movements across the tunnel alignment occurs (Figures 7.7 and 7.8). In addition, the forces and bending moments generated in the tunnel lining are also not symmetry as shown in Figure 7.18 to 7.32. These are the reasons that the full tunnel cross sections are necessary in each analysis.

As illustrated in Figures 7.19, 7.21, 7.24 and 7.30, the maximum of axial forces is generally located at the springline level on the side where the shortest pile foundations of the existing building are situated. The lower values of axial forces in the opposite side can be caused by the longer pile length of that side, which serves as a barrier to reduction of the lateral earth pressure.